Gas-Phase Condensation Reactions of SixOyHz- Oxyanions with H2O

ARTICLE *in* THE JOURNAL OF PHYSICAL CHEMISTRY A · SEPTEMBER 2001

Impact Factor: 2.69 · DOI: 10.1021/jp010905e

Gas-Phase Condensation Reactions of $Si_xO_yH_z^-$ Oxyanions with H_2O

G. S. Groenewold,* J. R. Scott, A. K. Gianotto, B. D. M. Hodges, G. F. Kessinger, and M. T. Benson

Idaho National Engineering and Environmental Laboratory, Idaho Falls, Idaho 83415

J. B. Wright

U. S. Army Soldier & Biological Chemical Command, Natick, Massachusetts 01760

Received: March 9, 2001; In Final Form: August 7, 2001

Water was reacted with gas-phase oxyanions having the general composition $Si_xO_yH_z^-$ that were formed and isolated in an ion trap-secondary ion mass spectrometer (IT-SIMS). The radical $SiO_2^{\bullet -}$ reacted slowly with H_2O to abstract $HO^\bullet$, forming SiO_3H^-, at a rate of 8×10^{-13} cm^3 molecule^{-1} s^{-1}, corresponding to an efficiency of about 0.03% compared with the theoretical collision rate constant (average dipole orientation). The product ion SiO_3H^- underwent a consecutive condensation reaction with H_2O to form $SiO_4H_3^-$ at a rate that was approximately 0.4−0.7% efficient. $SiO_4H_3^-$ did not undergo further reaction with water. The multiple reaction pathways by which radical $SiO_3^{\bullet -}$ reacted with H_2O were kinetically modeled using a stochastic approach. $SiO_3^{\bullet -}$ reacted with water by three parallel reaction pathways: (1) abstraction of a radical $H^\bullet$ to form SiO_3H^-, which then reacted with a second H_2O to form $SiO_4H_3^-$; (2) abstraction of a radical $OH^\bullet$ to form SiO_4H^-, which further reacted by consecutive $H^\bullet$ abstractions to form $SiO_4H_2^{\bullet -}$ and then $SiO_4H_3^-$; and (3) condensation with H_2O to form $SiO_4H_2^{\bullet -}$, which subsequently abstracted a radical $H^\bullet$ from a second H_2O to form $SiO_4H_3^-$. In all of these reactions, the rate constants were determined to be very slow, as determined by both direct measurement and stochastic modeling. For comparison, the even electron ion $Si_2O_5H^-$ was also investigated: it underwent condensation with H_2O to form $Si_2O_6H_3^-$, with a rate constant corresponding to 50% efficiency. The reactions were also modeled using ab initio calculations at the UB3LYP/6-311+G(2d,p) level. Addition of H_2O to $SiO_3^{\bullet -}$, SiO_3H^-, and $Si_2O_5H^-$ was calculated to be approximately 42, 45, and 55 kcal mol^{-1} exothermic, respectively, and encountered low activation barriers. Modeling of $SiO_2^{\bullet -}$ and $SiO_3^{\bullet -}$ reactions with H_2O failed to produce radical abstraction reaction pathways observed in the IT-SIMS, possibly indicating that alternative reaction mechanisms are operative.

I. Introduction

Silicon and water represent two of the most abundant components found on the surface of the earth. Aside from water, the earth's crust is estimated to be 57−60% SiO_2 (by weight).[1] As a result, interactions between silicate minerals and water are ubiquitous and central to our understanding of ongoing geologic and atmospheric processes.[2,3] It is well-known that water reactivity is influenced by the variable surface structure of silicon oxides.[4,5] For example, unstrained Si−O−Si moieties are strongly resistant to dissociative chemisorption.[6] In contrast, water is susceptible to chemisorption on reactive edge sites that are found on highly dehydroxylated silica, and these sites are the first to be hydroxylated upon initial exposure to water.[2] Subsequent interactions involve physisorption of molecular water to the hydroxylated silica surface, i.e., water is hydrogen-bonded to "dangling" O−H (silanol) moieties. A reflection of this change is that as the surface coverage of water increases, the enthalpy of adsorption decreases. The surface hydroxyl sites can have acidic or basic character,[6] and deprotonation of these sites results in formation of silicate oxyanions. These basic moieties are responsible for cation adsorption, and are also involved in water interaction.

Characterization of these interactions is quite challenging because of the heterogeneity of the surface sites and because it is difficult to separate the interactions that are solely surface phenomena from those related to the bulk of the material. Despite these difficulties, substantial information pertaining to silica structures have been realized using vibrational[6] and NMR spectroscopies.[7] Synchrotron-based X-ray techniques have provided remarkable insight into the chemical structure of silicate-based mineral surfaces.[8] Direct evaluation of the reactivity of the surface moieties, however, is a somewhat more difficult problem.

Examination of the individual surface moieties would provide an opportunity to study the surface−adsorbate interactions, but isolation in the condensed phase is not possible. An alternative approach is to isolate these moieties and study their interactions in the vapor phase. This has been accomplished in our laboratory by bombarding the sample surface with energetic projectiles, generally ReO_4^-.[9,10] Charged secondary ions derived from the sample surface can be trapped in an ion trap mass spectrometer, and their reactions with volatile neutral gases can be studied. This ion trap secondary ion mass spectrometry (IT-SIMS) approach enabled the investigation of the gas-phase reactions of $Al_xO_y^- + H_2O$, $AlO_x^- + H_2S$, and $SiO_xH_y^- + H_2S$.

The investigation of the reactions of aluminum oxyanions with water showed that AlO_2^- would slowly condense with two H_2O consecutively to form $AlO_3H_2^-$ and $AlO_4H_4^-$.[11] In contrast, $Al_2O_4H^-$ reacted with 100% efficiency to add a first H_2O. The product of the reaction, $Al_2O_4H_3^-$ reacted with ∼50% efficiency

10.1021/jp010905e CCC: $20.00
Published on Web 09/28/2001

to add a second H_2O. More recently, the reactions of AlO_2^-, $SiO_2^{\bullet-}$, $SiO_3^{\bullet-}$, and SiO_3H^- with H_2S were investigated.[12] These ions all reacted with H_2S at reaction rates that were 30−50% efficient. In the case of AlO_2^-, the reaction with H_2S was more than an order of magnitude faster than with H_2O, which was rationalized in terms of the higher gas-phase acidity of the neutral. The reaction pathway was also substantially different: AlO_2^- reacted with H_2S by consecutive (condensation−H_2O elimination) reactions, first forming $AlOS^-$ and then AlS_2^-. This reaction pathway was also observed for the reaction of SiO_3H^- with H_2S, first forming SiO_2SH^- and subsequently $SiOS_2H^-$. In contrast, the radical silicate anions $SiO_2^{\bullet-}$ and $SiO_3^{\bullet-}$ reacted with H_2S via radical abstraction.

In the current investigation, we sought to extend our knowledge of intrinsic Si oxyanion reactivity by systematically investigating the reactions of $Si_xO_yH_z^-$ ($x \leq 2$) with H_2O. The study revealed a suite of radical abstraction and condensation reactions. The $Si_1O_yH_z^-$ species were very slow and inefficient. In contrast, the condensation reaction of $Si_2O_5H^-$ was very fast. The results and interpretation of these studies are reported herein.

II. Experimental Section

Samples. Silica (5.24 m^2 g^{-1}) was obtained from the QuantaChrome Corporation (Syosset, NY). Powdered samples were attached to the end of a 2.7 mm probe tip with double-sided tape (3M, St. Paul, MN).

Instrumentation. The IT-SIMS instrument utilized in these studies has been described previously.[13−15] Briefly, this IT-SIMS is a modified Finnigan ITMS instrument (Finnigan Corp., San Jose, CA). Modifications include incorporation of a perrhenate (ReO_4^-) primary ion beam,[10] an insertion lock for introduction of solid samples, and an offset dynode with multichannel plate detector. The primary ion gun and sample probe tip are collinear and located outside opposite end caps of the ion trap. The primary ion gun was operated at 4.5 keV and produced a ReO_4^- beam with a 1.25 mm diameter at a primary ion current ranging from 300 to 600 pA. The ReO_4^- beam was used because this type of ion beam is more efficient for sputtering intact surface species into the gas phase than atomic particle bombardment.[16,17] The data acquisition and control system uses Teledyne Apogee ITMS Beta Build 18 software that controls routine ITMS functions and a Teledyne HST-1000 filtered noise field (FNF) system (Teledyne Electronic Technologies, Mountain View, CA). Data analysis was performed using SATURN 2000 software (version 1.4, Varian, Walnut Creek, CA).

For ion−molecule reaction experiments, H_2O vapor was admitted to the IT-SIMS after three freeze−pump−thaw cycles, via a variable leak valve. Pressures in these experiments ranged from $\sim 5 \times 10^{-7}$ to $\sim 3 \times 10^{-6}$ Torr. Ion gauge pressures were used without correction, because the ion gauge response for H_2O is nearly identical to that for N_2.[18] Helium bath gas was added to reach an operating pressure of 3×10^{-5} Torr (uncorrected). The IT-SIMS base pressure was 3×10^{-8} Torr.

IT-SIMS Parameters. Details of a representative sequence of events for ion−molecule reactions have been previously described.[11] In these experiments, the ion trap was operated with a low mass cutoff of 40 amu. Ionization times were adjusted so that a healthy population of ions (signal-to-noise $\geq \sim 100$) was generated. Ionization times ranged from ~50 to 200 ms, during which time the ReO_4^- beam was directed through the ion trap and onto the silica target. Ion isolation was performed at the same time as ionization (sample bombardment) by applying a notched FNF, where the frequencies of the notch corresponded to the natural frequency of the ion being isolated. This method results in ejection of ions whose natural frequencies do not fall within the notch. Since ion mass is correlated with frequency, mass selective ion isolation is accomplished.

Once the ions were formed and isolated, ion−molecule reactions with H_2O began to occur. Altering the duration of a delay period between the ionization/isolation event and the ion scan-out/detection event varied the extent of reaction.

After reaction, ions were scanned out of the ion trap using a mass selective instability scan with axial modulation.[19] To account for signal originating from grids on the ion trap end caps, background spectra were collected after each sample. Seven spectra (each composed of the average of 15 or 20 scans) were averaged and background-corrected to obtain final peak intensities. The relative standard deviation between averaged spectra was ±5%.

For any given experiment, ion lifetimes (the x axis on the kinetic plots) were estimated from the end of the ionization period to the exit of the ions from the trap. The FNF waveform is applied during the ionization period, ejecting all product ions formed during ionization. The delay period made up the majority of the ion lifetime, with corrections included for electronics stabilization and scanout (several milliseconds). The total experiment time was limited by the data systems to $\leq \sim 2$ s.

To generate kinetic plots, ion abundances were normalized to the sum of the reactant and product ions. The normalization corrected the data for a slow 10−20% apparent increase in ion abundances, which occurred as a result of increased trapping efficiency at longer delay periods. Approximately the same number of ions were generated in experiments that had short or long delay periods; however, at longer delay periods, the number of collisions with the He (3×10^{-5} Torr) bath gas was increased. This localized more ions in the center of the trap and improved the efficiency of the scanout and detection. This made the total number of ions in the trap appear to increase over the first 200 ms of the experiment.

Computational Methods. All ab initio molecular orbital calculations were performed on the $Si_xO_yH_z^- + H_2O$ systems using the *Gaussian98* program.[20] All structures were fully optimized using the UB3LYP exchange and correlation functionals[21,22] with the 6-311+G(2d,p) basis set. All minimizations were carried out using the Berny algorithm,[23,24] and the default parameters were used for the integral cutoff and minimization convergence criteria. Vibrational frequencies were calculated for all minima to ensure that the transition states had one imaginary frequency and all other minima had positive frequencies.

Calculation of Rate Constants. The reactions of $Si_xO_yH_z^-$ with H_2O was described using pseudo-first-order kinetics because the concentration of H_2O was significantly greater than the concentration of the ions produced and therefore remained essentially constant throughout the reaction. While the precision of the relative peak abundances between spectra was quite good (relative standard deviation of ±5%), more uncertainty was introduced due to pressure measurement of H_2O. Although the precision of H_2O pressure measurement was good, the absolute accuracy is somewhat uncertain, especially at low pressure. Experiments repeated at nearly equivalent H_2O pressures gave rate constants within ±30%, which was probably representative of the uncertainty in the pressure measurement. Therefore we concluded that the uncertainty in k_1^{exp} was approximately ±30%.

Reaction efficiency was evaluated by comparing measured rate constants with theoretical rate constants calculated using the reparametrized average-dipole-orientation (ADO) theory.[25] The reparametrized ADO constants were calculated using a

reaction temperature (310 K), which was the average ion temperature for an ion in a typical trap as calculated by both Goeringer[26] and Gronert.[27] These values were adopted in lieu of any direct temperature measurement or temperature control available on the IT-SIMS.

$SiO_2^{\bullet-}$ underwent consecutive reactions with H_2O. Although the rate constant for the initial reaction k_1 could be measured directly, the rate constants for subsequent reaction k_2 could only be estimated. The rate constant for the consecutive reactions was estimated using a stochastic kinetic modeling approach, based on a rigorously derived Monte Carlo procedure that numerically simulates the time evolution of the reactions.[28] The stochastic kinetic modeling was performed using the Chemical Kinetic Simulator ™ software package, that is available for downloading (with a no-cost license) on the IBM website.[29] The stochastic approach was adopted because it does not require exact solution of coupled differential equations required by the deterministic approach and, hence, is more adaptable to complicated kinetic systems, such as $SiO_3^{\bullet-} + H_2O$. $SiO_3^{\bullet-}$ undergoes consecutive, parallel reactions with H_2O, which were modeled with relative ease using the stochastic approach.

III. Results and Discussion

Bombarding silica particles with energetic projectiles generated the $Si_xO_yH_z^-$ species studied for reactivity with H_2O. The negative SIMS spectrum of silica[30] tends to be dominated by O^- and OH^-, but also contains low abundance ions corresponding to $SiO_2^{\bullet-}$, $SiO_3^{\bullet-}$, SiO_3H^-, and $Si_2O_5H^-$. These ions were mass-isolated, accumulated, and reacted in the IT-SIMS.

$SiO_2^{\bullet-}$. When $SiO_2^{\bullet-}$ (*m*/*z* 60) was isolated by the ion trap with a H_2O pressure of 2.5×10^{-6} Torr, a single reaction product was observed at *m*/*z* 77 after 16 ms (Figure 1). *m*/z 77 corresponded to SiO_3H^-, which arose by abstraction of an $OH^{\bullet}$ radical from H_2O (Reaction 1). This assignment was supported

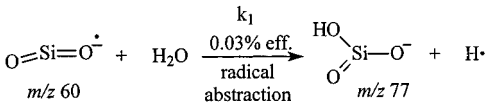

Reaction 1

by reaction of $SiO_2^{\bullet-}$ with D_2O, which resulted in formation of *m*/*z* 78, consistent with the expected composition SiO_3D^-.

As the reaction time was increased, a second reaction product appeared at *m*/*z* 95, which resulted from condensation of SiO_3H^- with H_2O to form $SiO_4H_3^-$ (Reaction 2). After approximately

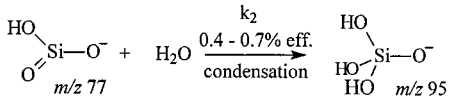

Reaction 2

500 ms, the abundance of $SiO_4H_3^-$ surpassed that of SiO_3H^-. The sequential relationship of the two ions was indicated by the kinetic plot (Figure 2): initially SiO_3H^- was more abundant, but it decreased as $SiO_4H_3^-$ increased. Compared with the average dipole orientation collision constant (k_{ADO}),[25] these reactions were very slow. After nearly 2 s reaction time (the limit of our ability to observe reactions in the IT-SIMS), the reaction was only 10% complete. However, we had no reason to believe that there was an unreactive ion population in the isolated *m*/*z* 60. Therefore, we concluded that $SiO_2^{\bullet-}$ was reacting with H_2O at a very slow rate. The exponential decrease in $SiO_2^{\bullet-}$ abundance enabled measurement of the apparent bimolecular rate constant (k_1) for the reaction of $SiO_2^{\bullet-} +$ H_2O: the measured value was 8×10^{-13} cm^3 molecule^{-1} s^{-1}, which made the reaction about 0.03% efficient compared with k_{ADO} (Table 1). The rate constant k_2 for the consecutive reaction of $SiO_3H^- + H_2O$ was estimated using the stochastic modeling

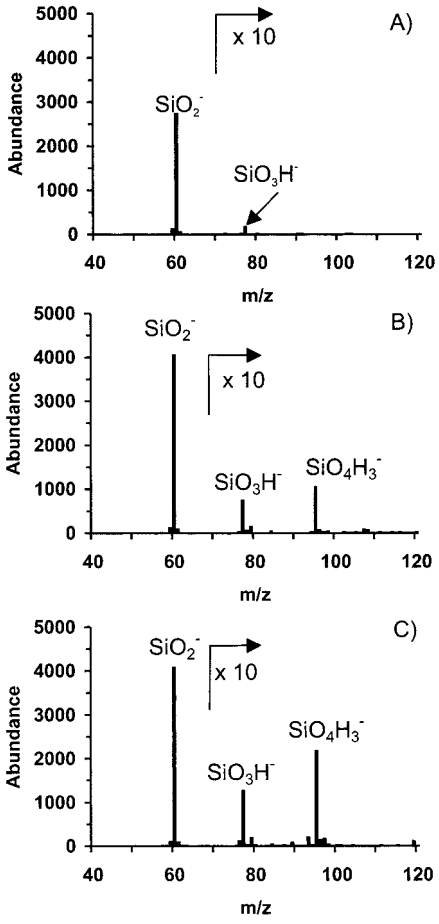

Figure 1. Reaction of isolated $SiO_2^{\bullet-}$ with H_2O after (A) 16, (B) 506, and (C) 1506 ms. Reaction can be seen to be progressing from $SiO_2^{\bullet-}$ (*m*/*z* 60) to SiO_3H^- (*m*/*z* 77) to $SiO_4H_3^-$ (*m*/*z* 95).

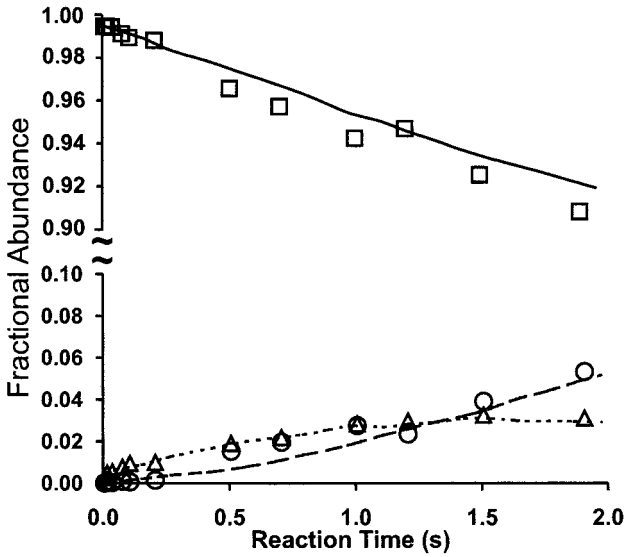

Figure 2. Fractional abundance versus reaction time for reaction of $SiO_2^{\bullet-} + H_2O \rightarrow SiO_3H^-$ and reaction $SiO_3H^- + H_2O \rightarrow SiO_4H_3^-$. Data and stochastic kinetic model are plotted. Fractional abundance scale is broken to show detail of reaction. □ $SiO_2^{\bullet-}$ data, − $SiO_2^{\bullet-}$ model, Δ SiO_3H^- data, ··· SiO_3H^- model, ○ $SiO_4H_3^-$ data, and - - - $SiO_4H_3^-$ model.

TABLE 1: Summary of Reaction Rate Constants for $Si_xO_yH_z^- + H_2O$

	reaction	$k_{experimental}$, cm^3 $molecule^{-1}$ s^{-1}	k_{ADO}, cm^3 $molecule^{-1}$ s^{-1}	reaction efficiency	comment
1	$SiO_2 + H_2O \rightarrow SiO_3H + H$	8×10^{-13}	2.4×10^{-9}	0.03%	directly measured
2	$SiO_3H + H_2O \rightarrow SiO_4H_3$	1.6×10^{-11}	2.3×10^{-9}	0.7%	stochastically modeled
		1.0×10^{-11}		0.4%	directly measured
3	$SiO_3 + H_2O \rightarrow SiO_3H + HO$	6×10^{-13}	2.3×10^{-9}	0.03%	stochastically modeled
4	$SiO_3 + H_2O \rightarrow SiO_4H + H$	1.4×10^{-12}	2.3×10^{-9}	0.06%	stochastically modeled
5	$SiO_3 + H_2O \rightarrow SiO_4H_2$	4×10^{-13}	2.3×10^{-9}	0.02%	stochastically modeled
6	$SiO_3H + H_2O \rightarrow SiO_4H_3$	1.0×10^{-11}	2.3×10^{-9}	0.4%	stochastically modeled
7	$SiO_4H + H_2O \rightarrow SiO_4H_2 + HO$	3.3×10^{-11}	2.3×10^{-9}	1.5%	stochastically modeled
8	$SiO_4H_2 + H_2O \rightarrow SiO_4H_3 + HO$	2.5×10^{-12}	2.3×10^{-9}	0.11%	stochastically modeled
9	$Si_2O_5H + H_2O \rightarrow Si_2O_6H_3$	1.2×10^{-9}	2.2×10^{-9}	50%	directly measured

approach: values of k_1 and k_2 were adjusted until a close fit to the data was obtained. This was achieved using a k_1 value of 6×10^{-13} cm^3 $molecule^{-1}$ s^{-1} and a k_2 value of 1.6×10^{-11}; the latter rate constant was 0.7% efficient compared with k_{ADO}. Note that SiO_3H^- reacted 30 times faster with H_2O than $SiO_2^{\bullet -}$. This behavior is reminiscent of the H_2O reactivity trend observed when comparing AlO_2^- with $AlO_3H_2^-$.[11]

These reactions, and others described in this paper, behave in a bimolecular fashion and can be accurately described using pseudo-first-order kinetics. However, we note that collisions with the He bath gas, which is needed in an ion trap to damp ion trajectories in the IT-SIMS, may serve to collisionally stabilize initially formed adducts, effectively making the reactions termolecular. The narrow range of operating pressures of the IT-SIMS [$(2-5) \times 10^{-5}$ Torr] do not facilitate careful evaluation of the role of the He bath gas in these reactions. Over the range of He pressures accessible, we were unable to observe significant variations in the measured reaction rates. This suggests that the initially formed adducts are not particularly sensitive to stabilization by thermal collisions with He. For this reason, we have chosen to describe these reactions using bimolecular rate constants.

SiO_3H^-. In addition to being formed from the reaction of H_2O with $SiO_2^{\bullet -}$, SiO_3H^- (*m*/*z* 77) was also sputtered into the ion trap SIMS directly from the silica surface. Isolation of SiO_3H^- followed by reaction with H_2O enabled the direct observation of the reaction pathway and measurement of the reaction kinetics. The results were consistent with the consecutive reaction starting from $SiO_2^{\bullet -}$ (above): SiO_3H^- was observed to undergo a single condensation reaction with H_2O to form $SiO_4H_3^-$ (Reaction 2, Figure 3). The rate constant for the exponential disappearance of SiO_3H^- was calculated at 1.0×10^{-11} cm^3 $molecule^{-1}$ s^{-1}. The reaction kinetics were stochastically modeled, which resulted in a good fit of the data if a rate constant of 1.2×10^{-11} cm^3 $molecule^{-1}$ s^{-1} was used in the model (Figure 4). The measured and modeled values are about 40% less than the rate constant estimated for the same reaction as it occurs consecutively starting from $SiO_2^{\bullet -}$. The reason for the discrepancy is not known, but may in part be due to the presence of the isobaric ion $^{29}SiO_3^{\bullet -}$, which would be isolated at *m*/*z* 77 with the predominant $^{28}SiO_3H^-$. Since $SiO_3^{\bullet -}$ reacts with H_2O about four to six times slower than SiO_3H^-, the ^{29}Si isotopic ion would make the observed rate slower than if only SiO_3H^- were present. A second explanation may be that SiO_3H^- formed from $SiO_2^{\bullet -}$ has more vibrational or kinetic energy, resulting in a somewhat faster reaction rate. These explanations notwithstanding, the difference in rates is not much greater than the estimated uncertainty in the concentration of H_2O. In any case, we feel that the salient conclusion derived from the study of the reaction of $SiO_3H^- + H_2O$ is that it is highly inefficient, being 0.4−0.7% of k_{ADO} (2.3×10^{-9} cm^3 $molecule^{-1}$ s^{-1}); it is, nevertheless, 20−30 times faster than the reaction of the radical $SiO_2^{\bullet -}$ with H_2O.

$SiO_3^{\bullet -}$. A third ion sputtered from the silica surface was the radical $SiO_3^{\bullet -}$, and when its reactivity with water was examined, more complex chemistry was observed. Product ions were observed at *m*/*z* 77, 93, 94, and 95 (Figure 5), which correspond to SiO_3H^-, SiO_4H^-, $SiO_4H_2^{\bullet -}$, and $SiO_4H_3^-$, respectively. This suite of product ions was best explained in terms of three parallel, consecutive reaction sequences. SiO_3H^-, SiO_4H^-, and

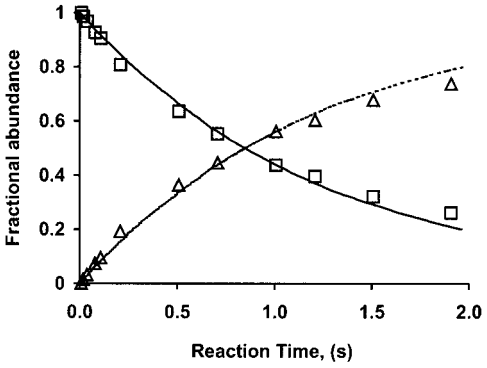

Figure 4. Fractional abundance versus reaction time for reaction of for $SiO_3H^- + H_2O \rightarrow SiO_4H_3^-$. □ SiO_3H^- data, − SiO_3H^- model, Δ $SiO_4H_3^-$data, and ··· $SiO_4H_3^-$ model.

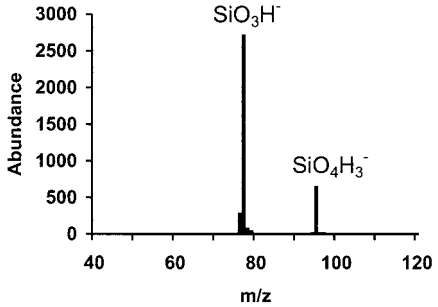

Figure 3. Mass spectrum of isolated SiO_3H^- (*m*/*z* 77) when reacted with H_2O to form $SiO_4H_3^-$ (*m*/*z* 95). Reaction time was 208 ms.

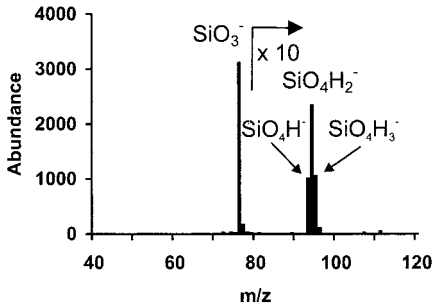

Figure 5. Mass spectrum of isolated $SiO_3^{\bullet -} + H_2O$. Reaction time was 708 ms.

$SiO_4H_2^-$ are probably formed directly from the reaction of $SiO_3^{\bullet -} + H_2O$ by $H^\bullet$ abstraction (k_3), $HO^\bullet$ abstraction (k_4), and H_2O condensation (k_5), respectively (Reactions 3−5). Hence

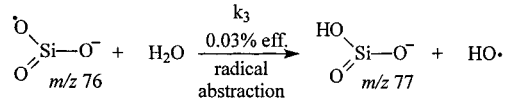

Reaction 3

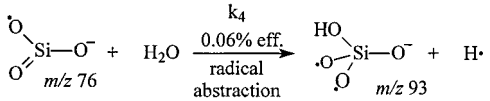

Reaction 4

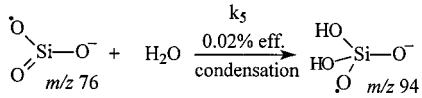

Reaction 5

the experimentally observed reaction constant k_{exp} for $SiO_3^{\bullet -} + H_2O$ must be equal to the sum of ($k_3 + k_4 + k_5$). The products of these reactions all undergo consecutive reactions with additional water molecules to produce the suite of product ions observed.

The consecutive reactions are either condensations or radical abstractions. As noted above, $SiO_3H^- + H_2O$ only results in condensation, producing $SiO_4H_3^-$ (Reaction 6, k_6). This ion does

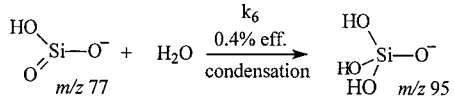

Reaction 6

not appear to react further. The reaction of $SiO_4H^- + H_2O$ only proceeds by $H^\bullet$ abstraction, producing $SiO_4H_2^{\bullet -}$ (Reaction 7,

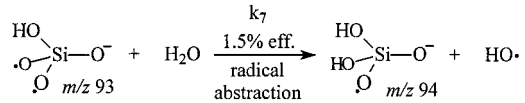

Reaction 7

k_7). Finally, $SiO_4H_2^{\bullet -} + H_2O$ reacts by $H^\bullet$ abstraction, producing $SiO_4H_3^-$ (Reaction 8, k_8).

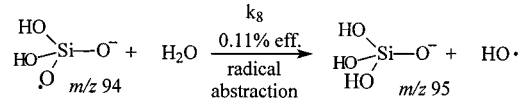

Reaction 8

To evaluate the relative contributions of these reactions, the reactions of $SiO_3^{\bullet -} + H_2O$ were stochastically modeled and compared with the kinetic plot (Figure 6). The best fit was achieved using six reactions (Reactions 3−8), by (a) constraining $\Sigma(k_3, k_4, k_5)$ to equal the measured disappearance constant for SiO_3^- (2.4×10^{-12} cm^3 molecule^{-1} s^{-1}) and (b) constraining k_6 to be within 30% of measured k_2 ($SiO_3H^- + H_2O \rightarrow SiO_4H_3^-$). The ratio of k_3 to k_4 to k_5 and the values for k_7 and k_8 were then varied to match the data points as closely as possible.

From this treatment, we estimated the relative rate constants, which were summarized in Table 1. The modeling indicated that the radical abstractions were more important than the H_2O condensation (behavior consistent with that of the radical $SiO_2^{\bullet -}$). In fact, a close fit to the data was also achieved *without* including the H_2O condensation reaction (Reaction 5), and the values for the rate constants were similar to those derived from the "six reaction" model. Hence the reaction to form $SiO_4H_2^{\bullet -}$ directly from $SiO_3^{\bullet -}$ by condensation with H_2O may not occur, but the best fit was achieved by including the H_2O condensation (Reaction 5).

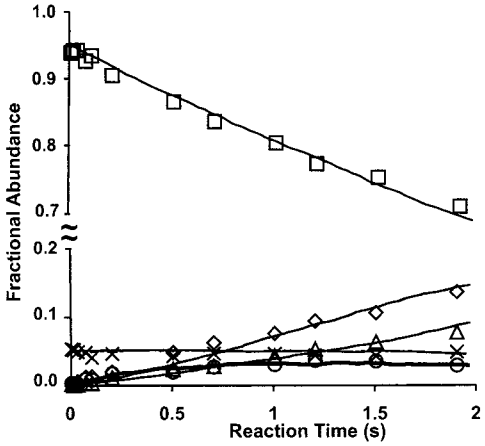

Figure 6. Fractional abundance versus reaction time for $SiO_3^{\bullet -} + H_2O$ data and six reaction model. Data points and associated stochastic kinetic models (–) are plotted. The fractional abundance scale is broken to show plot detail. □ $SiO_3^{\bullet -}$, × SiO_3H^-, ○ SiO_4H^-, ◇ $SiO_4H_2^{\bullet -}$, and Δ $SiO_4H_3^-$ data.

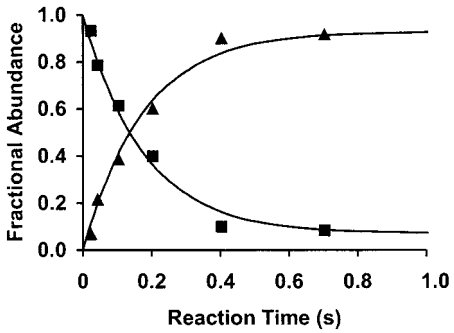

Figure 7. Kinetic plot of the experimental and stochastic modeled ion abundances versus time for the reaction of $Si_2O_5H^- + H_2O \rightarrow Si_2O_6H_3^-$. ■ $Si_2O_5H^-$ data, – $Si_2O_5H^-$ model, ▲ $Si_2O_6H_3^-$data, and – $Si_2O_6H_3^-$ model.

The other reaction pathway for formation of $SiO_4H_2^{\bullet -}$ is from SiO_4H^- by $H^\bullet$ abstraction. This reaction appears to be notably faster than other reactions in this series. Structural possibilities for SiO_4H^- include both diradical and peroxy structures; the diradical is preferred in this case, because radical Si oxyanions in general react by radical abstraction. The resulting product $SiO_4H_2^{\bullet -}$ is also a radical anion and reacts by $H^\bullet$ abstraction to form the end product, $SiO_4H_3^-$.

$Si_2O_5H^-$. The ion observed at *m*/*z* 137 in the SIMS spectrum of silica corresponds to $Si_2O_5H^-$. It was isolated and underwent a rapid condensation reaction with H_2O to form $Si_2O_6H_3^-$ at *m*/*z* 155 (Reaction 9, Figure 7). The exponential decay of the $Si_2O_5H^-$ abundance enabled the rate constant to be calculated at 1.2×10^{-10} cm^3 molecule^{-1} s^{-1}, which corresponded to approximately 50% efficiency compared with k_{ADO}. This rate is dramatically faster than the rate measured for the water condensation of SiO_3H^-. By comparing SiO_3H^- to $Si_2O_5H^-$, the large increase in reactivity was reminiscent of a similar increase observed when comparing the H_2O reactivity of AlO_2^-

and $AlO_3H_2^-$ (efficiencies of 2−3%) with that of $Al_2O_4^-$ (100% efficiency).[11]

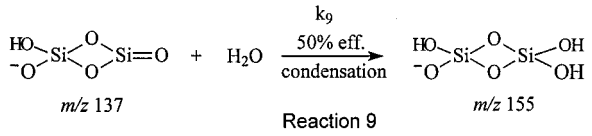

Reaction 9

Ab Initio Calculations. *$SiO_2^{\bullet-}$*. Structures and reaction pathways were modeled at the UB3LYP/6-311+G(2d,p) level to attempt to understand plausible mechanisms for the silicate oxyanion reactions. Initially, we attempted to model the reaction of the radical $SiO_2^{\bullet-} + H_2O$; however, all attempts to do this resulted in formation of $SiO_3H_2^{\bullet-}$, which was not experimentally observed. It appears that the experimentally observed product results in the generation of $H^\bullet$, which has a significant enthalpy of formation, which makes the observed chemistry unfavorable if it is assumed that the reactants are in thermal equilibrium with the surroundings. If, however, some fraction of the reacting $SiO_2^{\bullet-}$ in the ion trap was significantly more energetic than 310 K, this might enable a net endothermic reaction to proceed. Certainly, a significant fraction of the $SiO_2^{\bullet-}$ is liable to be formed during the SIMS bombardment in hyperthermal kinetic and internal energy states; however, the temperature and internal energy of the reacting ions are unknown, and hence we cannot do anymore than speculate on this possibility given the limitations of the current IT-SIMS approach.

A second hypotheses considered in an attempt to reconcile the experimental and modeling results included the possible participation of a second H_2O molecule, which might stabilize the departing $H^\bullet$ radical. This is similar to modeling results of surface silanol moieties, which are most stable when coordinated by two H_2O molecules.[2] However, this possibility was rejected in the present case because it was not supported by the bimolecular nature of the kinetics.

The fact that the ab initio calculations did not successfully replicate the reaction pathway for $SiO_2^{\bullet-} + H_2O$ serves as a caveat for the application of the calculations to the systems subsequently described. We have nevertheless chosen to include the calculations because (a) they successfully predict reaction pathways for the closed-shell ions SiO_3H^- and $Si_2O_5H^-$, (b) the results for the closed-shell ions are self-consistent with previous results for closed-shell ions,[11,12] and (c) it is hoped that more elegant ion chemistry and or improved calculations will be applied to the open-shell systems.

$SiO_3^{\bullet-}$. When the reaction of radical $SiO_3^{\bullet-}$ with H_2O was calculated, the reactions showed exothermic formation of the condensation product $SiO_4H_2^-$ (*m/z* 94, above) with low barriers (Figures 8 and 9). The reaction is initiated by formation of a H-bound adduct and proceeded through a rhomboid transition state in which the H−OH bond is broken and a HO−Si bond is formed. This result is very similar to earlier ab initio results that modeled the hydrolysis of Si−O moieties.[31,32] As in the case of $SiO_2^{\bullet-}$, current computational support could not be generated for the radical abstraction reactions of $SiO_3^{\bullet-} + H_2O$ (forming $SiO_3H^- + OH^\bullet$ and $SiO_4H^- + H^\bullet$).

SiO_3H^-. Calculations of condensation reactions involving the even electron silicate anions yielded results consistent with experiments. When SiO_3H^- reacts with H_2O, it was found initially to form a H-bound adduct (Figures 10 and 11). The adduct then encountered a barrier of nearly 12 kcal mol^{-1}, in which the H−OH bond is broken, and a HO−Si bond is formed. The reaction was net 45 kcal mol^{-1} exothermic, which is in reasonable agreement with the ΔH_f of the Si−O bond in quartz (54 kcal mol^{-1},[2]).

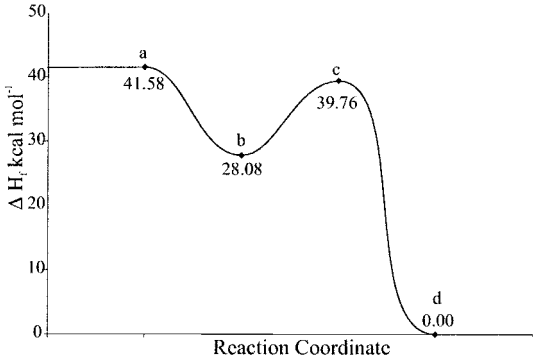

Figure 8. Reaction coordinate diagram for $SiO_3^- + H_2O \rightarrow SiO_4H_2^-$. Relative ΔH_f values were calculated at the UB3LYP/6−311+G(2d,p) level of theory structures corresponding to the reactants (a), the initial H-bound adduct (b), the transition state (c), and the product ion (d); see Figure 9.

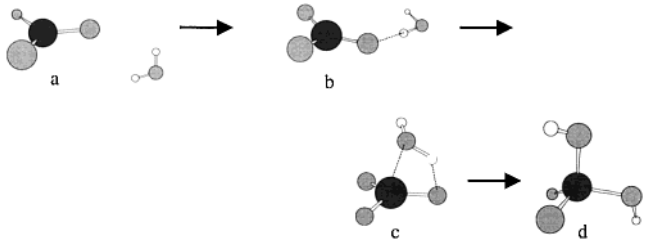

Figure 9. Calculated reaction mechanism for $SiO_3^- + H_2O \rightarrow SiO_4H_2^-$. Structures were calculated at the UB3LYP/6−311+G(2d,p) level of theory.

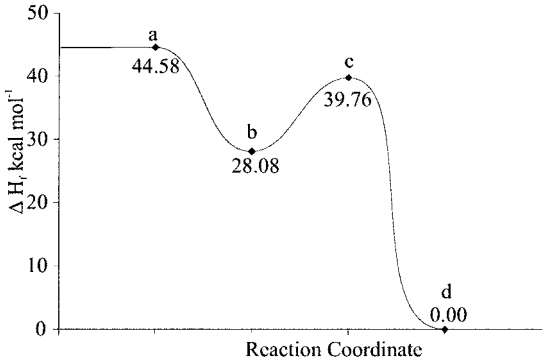

Figure 10. Reaction coordinate diagram for $SiO_3H^- + H_2O \rightarrow SiO_4H_3^-$. Relative ΔH_f values were calculated at the UB3LYP/6−311+G(2d,p) level of theory structures corresponding to the reactants (a), the initial H-bound adduct (b), the transition state (c), and the product ion (d); see Figure 11.

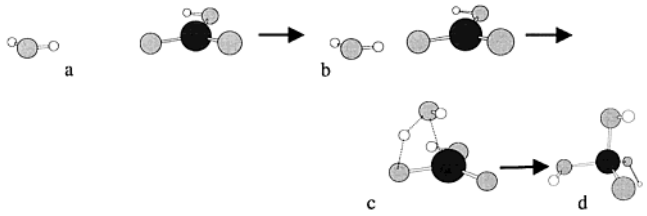

Figure 11. Calculated reaction mechanism for $SiO_3H^- + H_2O \rightarrow SiO_4H_3^-$. Structures were calculated at the UB3LYP/6−311+G(2d,p) level of theory.

$Si_2O_5H^-$. Ab initio calculations for the $Si_2O_5H^- + H_2O$ system revealed that the structure of the reactant anion was a four-membered disilacycle with two dangling oxygen atoms and a hydroxyl (Figure 12), with electron density being concentrated on the dangling oxygens. Acyclic structural alternatives were predicted to be unstable. When $Si_2O_5H^-$ reacted with H_2O, two

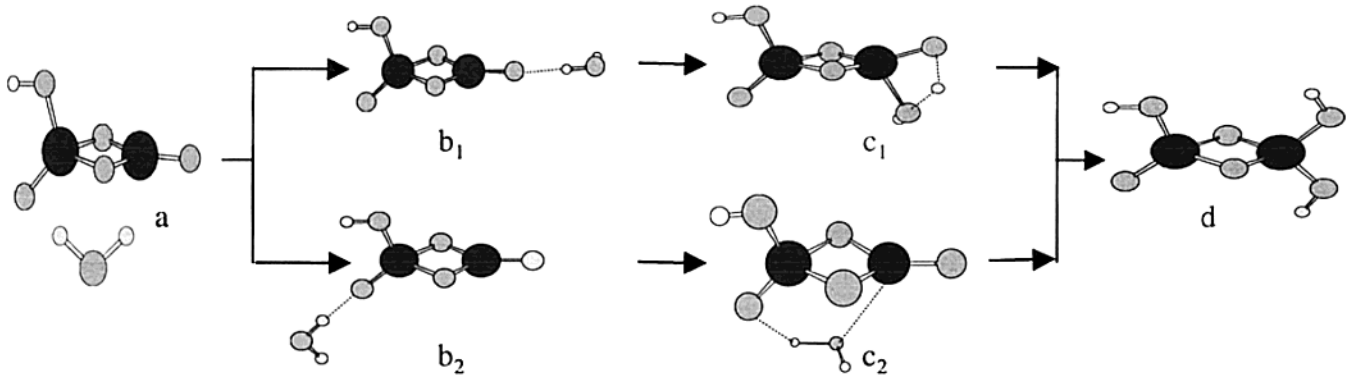

Figure 12. Calculated reaction mechanism for $Si_2O_5H^- + H_2O \rightarrow Si_2O_6H_3^-$. Structures were calculated at the UB3LYP/6−311+G(2d,p) level of theory.

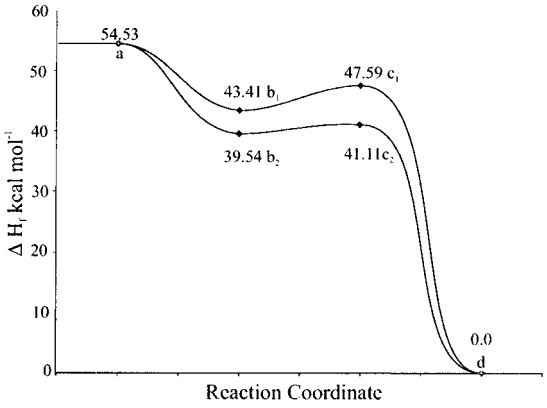

Figure 13. Reaction coordinate diagram for $Si_2O_5H^- + H_2O \rightarrow Si_2O_6H_3^-$. Relative ΔH_f values calculated at the UB3LYP/6−311 + G(2d,p) level of theory. Two energetically competitive reaction pathways were identified starting from reactants (a), leading to formation of two possible H-bound adducts (b_1 and b_2), proceeding through two possible transition states (c_1 and c_2), and finally generating the product ion (d). See Figure 12.

energetically competitive H-bound adducts were identified: these corresponded to hydrogen-bound water at either of the two dangling oxygen atoms. Adduct formation with the tetrahedral Si−O (b_2) was slightly more exothermic, and proceeded through a very low transition state (c_2, ∼1.5 kcal mol^{-1}) in which the OH is transferred across the disilacycle (Figure 13). However initial adduct formation with the trigonal Si−O (b_1) was also energetically favorable, although the transition state barrier was slightly higher (c_1, ∼4 kcal mol^{-1}). Hence, we preferred the a → b_2 → c_2 → d mechanism, while acknowledging that the energy values are close enough that both mechanisms are viable possibilities. It was noteworthy that both mechanisms produced the same $Si_2O_6H_3^-$ product structure, and that the reactions were exothermic by 55 kcal mol^{-1}, which, as noted above, was in excellent agreement with the ΔH_f of the Si−O bond.

Reactivity Comparisons. The vast difference in the reaction kinetics of $Si_2O_5H^- + H_2O$ condensation compared with SiO_3H^- begs explanation. Both ions form H-bound adducts apparently without barrier. Once formed, however, the transition state encountered by the $SiO_3H^- - H_2O$ adduct is significantly larger than that encountered by the $Si_2O_5H^-$ adduct, and this difference could explain the kinetic differences observed. However, our previous research with $Al_xO_yH_z^- + H_2O$, barrier height did not strongly correlate with observed differences in reaction efficiencies. Alternatively, we had previously noted a marked difference in dipole moment, when $AlO_xH_y^- + H_2O$ was compared with that of $Al_2O_xH_y^-$.[11] In this study, the condensations $Al_2O_4H^-$ and $Al_2O_5H_2^-$ were 100% and 50% efficient, respectively, compared to the more inefficient condensations of the $Al_1O_xH_y^-$ species, and it had been suggested that this may correlate with marked differences in *ion* dipole moments. We speculated that the dipole of the ion may preorient the molecule, thus improving the probability of a reactive collision. This also may be a factor in the present case.

The present study also enables comparison of the intrinsic H_2O reactivity of Si oxyanions with their Al counterparts. In comparing the reactivity of AlO_2^- with that of $SiO_2^{\bullet -}$, we observe that the former is much more reactive: the efficiency of AlO_2^- is 2%, nearly 100 times more efficient than $SiO_2^{\bullet -}$ (only 0.03%). We note that AlO_2^- reacts by condensation, as contrasted with the radical $SiO_2^{\bullet -}$ which reacts by $OH^\bullet$ abstraction.

In a similar vein, SiO_3H^- is much less reactive with H_2O than is $AlO_3H_2^-$. Both ions react with H_2O by condensation; however, the efficiency of the $AlO_3H_2^-$ condensation is 20%, which is 20 to 30 times more efficient than that SiO_3H^-.

In contrast to the marked differences observed when comparing the reactivity of the Al_1- with the Si_1-oxyanions, H_2O reactivity with the of the Si_2- and Al_2- oxyanions are comparable. The condensation efficiency of $Si_2O_5H^-$ is nearly identical to that of $Al_2O_5H_3^-$, but somewhat lower as compared with the efficiency of $Al_2O_4H^-$. These differences strongly recommend pursuing an evaluation of the H_2O reactivity of larger aluminate and silicate anions; however, generation of these ions using SIMS has proven somewhat difficult. It may be that laser desorption of these ions would be more practical, as suggested by the research of Lafargue.[33]

The present research also allows the reactions of $SiO_xH_y^- + H_2O$ to be compared with previous reactivity studies with H_2S.[12] Generally speaking, reactions with H_2S are orders of magnitude more efficient than reactions with H_2O, which may be explained simply in terms of the much greater gas-phase acidity of H_2S compared to H_2O.[34] For example, $SiO_2^{\bullet -}$ reacts with both H_2O and H_2S by radical abstraction (OH in the case of H_2O and SH in the case of H_2S); however, the H_2S reaction is 1000 times more efficient than the H_2O reaction. A similar difference in reaction efficiencies exists in the case of $SiO_3^{\bullet -}$: this ion abstracts a H radical from both H_2O and H_2S, but the reaction is more than 1000 times more efficient in the latter case.

Differences in H_2S versus H_2O reaction efficiencies for SiO_3H^- are not quite as large, although reaction with H_2S is 30 to 70 times more efficient than reaction with H_2O. However, the reaction mechanism is quite different in this comparison: SiO_3H^- reacts with H_2O by condensation to form tetracoordinate $SiO_4H_3^-$, whereas SiO_3H^- undergoes O-for-S exchange to form SiO_2SH^- when reacting with H_2S.

Conclusions

The reactions of small $Si_xO_yH_z^-$ anions with H_2O were evaluated using an ion trap secondary ion mass spectrometry (IT-SIMS) approach and shown to display a range of reactivity behavior. The smallest anions studied, $SiO_yH_z^-$, reacted very slowly, which implied that most of the interactions did not result in reaction. In the case of the even electron anions, condensation was the preferred pathway; however, for the radicals, radical abstraction generally occurred. In marked contrast, the even electron $Si_2O_5H^-$ underwent condensation on nearly every collision. Ab initio calculations revealed the existence of very low barriers in this latter case, which may be related to the efficient condensation reactions observed.

These results are promising in that they demonstrate that a wide range of intrinsic reactivity information can be generated for oxyanion moieties. However, fulfillment of the promise of the approach clearly points toward investigation of the reactivity of larger and more complex oxyanion moieties. Hence, future research must focus on the generation and characterization of such larger mineral oxyanions and ways to investigate them in more extensively hydrated forms.

Acknowledgment. This research was supported by the United States Department of Energy, under Contract DE-AC07-99ID13727 BBWI.

Supporting Information Available: Spectra for the reaction of $Si_2O_5H^- + H_2O \rightarrow Si_2O_6H_3^-$ at 2.0×10^{-7} Torr H_2O acquired after (A) no delay, showing $Si_2O_5H^-$ (*m*/*z* 137) and a small amount of $Si_2O_6H_3^-$ (*m*/*z* 155); (B) 20 ms, where the formation of $Si_2O_6H_3^-$ becomes evident; (C) 180 ms; (D) 380 ms; and (E) 680 ms, in which the ion population has been nearly entirely converted to $Si_2O_6H_3^-$ (*m*/*z* 155). This material is available free of charge via the Internet at http://pubs.acs.org.

References and Notes

(1) Faure, G. *Principles and Applications of Inorganic Geochemistry*; MacMillan Publishing Company: New York, 1991.

(2) Dove, P. M.; Rimstidt, J. D. Silica-Water Interactions. In *Silica Physical Behavior, Geochemistry and Materials Applications*; Heaney, P. J., Prewitt, C. T., Gibbs, G. V., Eds.; Mineralogical Society of America: Washington, DC, 1994; Vol. 29; pp 259−308.

(3) Grillet, Y.; Llewellyn, P. L. Adsorption Properties of the Silica Surface. In *The Surface Properties of Silicas*; Legrand, A. P., Ed.; John Wiley & Sons: New York, 1998; pp 24−81.

(4) Iler, R. K. *The Chemistry of Silica: Solubility, Polymerization, Colloid and Surface Properties, and Biochemistry*; John Wiley & Sons: New York, 1979.

(5) Legrand, A. P. On the Silica Edge. In *The Surface Properties of Silicas*; Legrand, A. P., Ed.; John Wiley & Sons: New York, 1998; pp 1−19.

(6) Burneau, A. G.; Gallas, J.-P. Vibrational Spectroscopies. In *The Surface Properties of Silicas*; Legrand, A. P., Ed.; John Wiley & Sons: New York, 1998; pp 147−234.

(7) Hommel, H.; Legrand, A. P.; Doremieux, C.; d'Espinose de la Callerie, J.-B. NMR Spectroscopies. In *The Surface Properties of Silicas*; Legrand, A. P., Ed.; John Wiley & Sons: Chichester, 1998; pp 470.

(8) Conradson, S. D. *Appl. Spectrosc.* **1998**, *52*, 252A-279A.

(9) Groenewold, G. S.; Kessinger, G. F.; Scott, J. R.; Gianotto, A. K.; Appelhans, A. D.; Delmore, J. E. *Anal. Chem.* **2001**, *73*, 226−232.

(10) Delmore, J. E.; Appelhans, A. D.; Peterson, E. S. *Int. J. Mass Spectrom. Ion Processes* **1995**, *146/147*, 15−20.

(11) Scott, J. R.; Groenewold, G. S.; Gianotto, A. K.; Benson, M. T.; Wright, J. B. *J. Phys. Chem. A* **2000**, *104*, 7079−90.

(12) Groenewold, G. S.; Hodges, B. D. M.; Scott, J. R.; Gianotto, A. K.; Appelhans, A. D.; Wright, J. B. *J. Phys. Chem. A* **2001**, *105*, 4059−4064.

(13) Ingram, J. C.; Appelhans, A. D.; Groenewold, G. S. *Int. J. Mass Spectrom. Ion Processes* **1998**, *175*, 253−62.

(14) Groenewold, G. S.; Appelhans, A. D.; Ingram, J. C. *J. Am. Soc. Mass Spectrom.* **1998**, *9*, 35−41.

(15) Groenewold, G. S.; Appelhans, A. D.; Ingram, J. C.; Gresham, G. L.; Gianotto, A. K. *Talanta* **1998**, *47*, 981−986.

(16) Appelhans, A. D.; Delmore, J. E. *Anal. Chem.* **1989**, *61*, 1087−93.

(17) Groenewold, G. S.; Delmore, J. E.; Olson, J. E.; Appelhans, A. D.; Ingram, J. C.; Dahl, D. A. *Int. J. Mass Spectrom. Ion Processes* **1997**, *163*, 185−195.

(18) Bartmess, J. E.; Georgiadis, R. M. *Vacuum* **1983**, *33*, 149−153.

(19) *Practical Aspects of Ion Trap Mass Spectrometry*; Todd, J. F. J., Ed.; CRC Press: New York, 1995; Vol. 1, p 4.

(20) Frisch, M. J.; Trucks, G. W.; Schlegel, H. B.; Scuseria, G. E.; Robb, M. A.; Cheeseman, J. R.; Zakrzewski, V. G.; Montgomery, J. A. Jr.; Stratmann, R. E.; Burant, J. C.; Dapprich, S.; Millam, J. M.; Daniels, A. D.; Kudin, K. N.; Strain, M. C.; Farkas, O.; Tomasi, J.; Barone, V.; Cossi, M.; Cammi, R.; Mennucci, B.; Pomelli, C.; Adamo, C.; Clifford, S.; Ochterski, J.; Petersson, G. A.; Ayala, P. Y.; Cui, Q.; Morokuma, K.; Malick, D. K.; Rabuck, A. D.; Raghavachari, K.; Foresman, J. B.; Cioslowski, J.; Ortiz, J. V.; Stefanov, B. B.; Liu, G.; Liashenko, A.; Piskorz, P.; Komaromi, I.; Gomperts, R.; Martin, R. L.; Fox, D. J.; Keith, T.; Al-Laham, M. A.; Peng, C. Y.; Nanayakkara, A.; Gonzalez, C.; Challacombe, M.; Gill, P. M. W.; Johnson, B.; Chen, W.; Wong, M. W.; Andres, J. L.; Gonzalez, C.; Head-Gordon, M.; Replogle, E. S.; Pople, J. A. *Gaussion98*, rev. A.4; Gaussian, Inc.: Pittsburgh, PA, 1998.

(21) Becke, A. D. *J. Chem. Phys.* **1993**, *98*, 5648.

(22) Lee, C.; Yang, W.; Parr, R. *Phys. Rev. B: Condens. Matter* **1988**, *37*, 785.

(23) Peng, C. *Israel J. Chem.* **1994**, *33*, 449.

(24) Peng, C. *J. Comput. Chem.* **1996**, *17*, 49.

(25) Su, T.; Chesnavich, W. J. *J. Chem. Phys.* **1982**, *76*, 5183−5185.

(26) Goeringer, D. E.; McLuckey, S. A. *Int. J. Mass Spectrom. Ion Processes* **1998**, *177*, 163−74.

(27) Gronert, S. *J. Am. Soc. Mass Spectrom.* **1998**, *8*, 845−8.

(28) Gillespie, D. T. *J. Phys. Chem.* **1977**, *81*, 2340−60.

(29) Houle, F. A.; Hinsberg, W. D. *Surf. Sci.* **1985**, *338*, 329.

(30) Vickerman, J. C.; Briggs, D.; Henderson, A. *The Static SIMS Library*; Surface Spectra Ltd.: Manchester, UK, 1999.

(31) Xiao, Y.; Lasaga, A. C. *Geochim. et Cosmochim. Acta* **1994**, *58*, 5379−5400.

(32) Gibbs, G. V.; Lasaga, A. C. *Am. J. Sci.* **1990**, *290*, 263−295.

(33) Lafargue, P. E.; Gaumet, J. J.; Muller, J. F.; Labrosse, A. *J. Mass Spectrom.* **1996**, *31*, 623−632.

(34) Lias, S. G.; Bartmess, J. E.; Liebman, J. F.; Holmes, J. L.; Levin, R. D.; Mallard, W. G. Ion Energetics Data. In *NIST Chemistry WebBook*, NIST Standard Reference Database Number 69, February 2000; Mallard, W. G., Linstrom, P. J., Eds.; National Institute of Standards and Technology: Gaithersburg MD, 20899, 2000; (http://webbook.nist.gov).